nanomanufacturing

MDPI

Article

Influence of γ-Irradiation on the Electronic Structure and the Chemical and Mechanical Properties of Poly(hydroxybutyrate-valerate)/Poly(caprolactone) Blends: Insights from Experimental Data and Computational Approaches

Francisco Rosario [1], João Paulo Almirão de Jesus [2], Suzan Aline Casarin [3] and Felipe de Almeida La Porta [2,4,*]

[1] Department of Materials Science and Engineering, Federal University of Technology—Paraná, Londrina 86036–370, Paraná, Brazil; rosario@utfpr.edu.br
[2] Post-Graduation Program in Chemistry, State University of Londrina, Rodovia Celso Garcia Cid, 445, km 380, Londrina 86057-970, Paraná, Brazil; joao.paulo.almirao@uel.br
[3] Department of Materials Science and Engineering, Federal University of São Carlos, Rod. Washington Luiz, s/n—Monjolinho, São Carlos 13565-905, São Paulo, Brazil; suzancasarin@ufscar.br
[4] Laboratory of Nanotechnology and Computational Chemistry, Department of Chemistry, Federal University of Technology—Paraná, Londrina 86036–370, Paraná, Brazil
* Correspondence: felipelaporta@utfpr.edu.br

Abstract: In this study, we investigated the influence of γ-irradiation (0, 50, and 100 kGy) doses on the chemical and mechanical properties of biodegradable poly(hydroxybutyrate-valerate)/poly (caprolactone) (PHBV/PCL) polymer blends rich in low-molar-mass PCL, which were prepared using a co-rotating twin-screw extruder. In parallel, the density functional theory (DFT) and the time-dependent DFT (TD-DFT) methods were used together with a model containing four monomer units to provide an insight into the electronic structure, chemical bonds, and spectroscopic (such as Nuclear Magnetic Resonance (NMR) and Ultraviolet-visible (UV-vis)) properties of PHBV and PCL blend phases, which are critical for predicting and designing new materials with desired properties. We found that an increase in γ-irradiation doses caused splitting instead of crosslinks in the polymer chains, which led to evident deformation and an increase in tensile strength at break of 2.0 to 5.7 MPa for the PHBV/PCL blend. Further, this led to a decrease in crystallinity and proved the occurrence of a more favorable interaction between the blend phases.

Keywords: poly(hydroxybutyrate-valerate); poly(caprolactone); polymer blends; chemical and mechanical properties; γ-irradiation doses; electronic structure calculations

Citation: Rosario, F.; Almirão de Jesus, J.P.; Casarin, S.A.; La Porta, F.d.A. Influence of γ-Irradiation on the Electronic Structure and the Chemical and Mechanical Properties of Poly(hydroxybutyrate-valerate)/Poly(caprolactone) Blends: Insights from Experimental Data and Computational Approaches. *Nanomanufacturing* **2024**, *4*, 27–44. https://doi.org/10.3390/nanomanufacturing4010002

Academic Editor: Asterios (Stergios) Pispas

Received: 26 September 2023
Revised: 8 December 2023
Accepted: 21 December 2023
Published: 10 January 2024

1. Introduction

Recently, biodegradable polymer blend systems have received significant attention in many biomedical applications (e.g., in controlled drug release systems, suture materials, and orthopedic implants) owing to their novel physicochemical properties [1–4]. Notably, the miscibility of prepared polymer blends is a determinant of their properties and functionalities [1,5–7]. For instance, miscible blends usually exhibit a single-phase morphology, which leads to reproducible mechanical properties. Contrarily, immiscible blends exhibit significant morphological heterogeneity, which leads to irreproducible physicochemical properties [1–9].

Various synthesis strategies (e.g., chemoenzymatic methods, enzymatic ring opening polymerization, radical ring opening polymerization, coordinative ring opening polymerization, anionic ring opening polymerization, photo-initiated ring opening polymerization, and so on) have been widely employed in the preparation of a diverse mixture of biodegradable polymer blends with different compositions, phases, and morphologies [7,9–17]. Among biodegradable polymeric blends, more recently, poly(hydroxybutyrate-valerate)

(PHBV) and poly(caprolactone) (PCL) have garnered extensive interest concerning a wide range of technological applications, thereby providing opportunities to develop emergent technologies in the future [18–22]. In particular, PHBV is a copolymer of hydroxybutyrate and valerate monomers and has several interesting properties that make it useful for a variety of applications. For example, it has a high melting point (above 160 °C) and is crystalline in nature, giving it good mechanical properties such as high tensile strength and modulus [23–25]. One of the main applications of PHBV is in the production of biodegradable plastics [26]. These plastics based on PHBV can be used in a variety of applications where traditional petroleum-based plastics would normally be used, but can be broken down by microorganisms over time, reducing the environmental impact of their use [27–29]. PHBV can also be used to make films, fibers, and other products [30]. Other potential applications of PHBV, more recently explored in the literature, include its use in drug delivery systems, tissue engineering, and as a material for 3D printing [31–37]. However, it is well-known that the large-scale production of these biopolymers occurs mainly through a bacterial fermentation process, which remains somewhat costly [38–41]. A rational strategy to reduce production costs and modify the physicochemical properties and degradation rates of such blends is of high value [1,2,42].

On the other hand, PCL is a biodegradable petroleum-based polymer, linear polyester with a low melting temperature (around 65 °C) and good mechanical properties [43–45]. However, it is well-known that several microbial enzymes, including esterase, cutinase, and lipase, can efficiently break down PCL into valuable chemicals [46–49]. In addition, the hydrolytic degradation rate of PCL is significantly slow, most likely due to its well-known hydrophobic nature [50,51]. It is also biocompatible, making it suitable for use in medical and pharmaceutical applications [52–55]. When blended, PHBV and PCL can form materials with a range of mechanical and thermal properties, depending on the blend ratio. It has been found that an increase in PHBV within the PCL matrix leads to a marked decrease in its miscibility [56]. In terms of mechanical properties, PHBV/PCL blends have a combination of the properties of the individual polymers. For example, PHBV has a high melting point and good mechanical properties such as high tensile strength and modulus, while PCL has a lower melting point and good flexibility [57,58]. As a result, PHBV/PCL blends can have a balance of high strength and good flexibility, as well as biodegradability, depending on the ratio of the two polymers in the blend.

For instance, Liu et al. have studied the biodegradation assay of PHBV/PCL blends using Pseudomonas mendocina [59]. After 96 h of degradation, the PHBV blends undergo extensive decomposition, leaving behind several channel-like structures, while the PCL portion remains apparently intact. Notably, it is well-known that the PCL polymer degrades over months to years depending on its molecular weight, degree of crystallinity, morphology, porosity, and the surrounding environment [22,60–62].

In some cases, biodegradable polymers may be used in applications where they will be exposed to γ-radiation, such as in medical devices or food packaging [63,64]. It has been observed that using ionized radiation during the processing of these systems improves thermal stability, miscibility, and other relevant properties [18,65,66]. Furthermore, in the polymers that undergo crosslinking when subjected to ionizing radiation, chemical bonds are formed between adjacent molecules, which lead to permanent linking [67]. In these cases, it is important to understand how the polymer will be affected by the radiation to ensure that it will still function as intended. The specific effects of γ-radiation on the chemical and mechanical properties of particular biodegradable polymer blends will depend on the structure and composition of each polymer, as well as the specific conditions under which they are irradiated [68–71]. However, the effects of γ-radiation doses on the chemical and mechanical properties of biodegradable PHBV/PCL polymeric blends remain to be elucidated.

Herein, we have tried to understand further the effects of γ-radiation (0, 50, and 100 kGy) doses on the chemical and mechanical properties of PHBV/PCL (25:75) systems rich in low molar mass PCL and prepared by means of a co-rotating twin-screw extruder.

This 25:75 ratio for the PHBV/PCL blend is due to its optimal suitability for biomedical applications. These blends were characterized using scanning electron microscopy (SEM), differential scanning calorimetry (DSC), dynamic mechanical thermal analysis (DMTA), and mechanical tensile tests, together with computational studies based on density functional theory (DFT) and time-dependent DFT (TD-DFT). By combining theoretical simulations with experimental techniques, it is possible to better understand the interaction between polymer blends and to predict their stability, reactivity, and spectroscopic behavior in different applications. Additionally, to elucidate the mechanical response of these systems, we evaluated the elastic modulus of these samples by changing the doses of γ-irradiation. Notably, the experimental results revealed the general degradation mechanism of these PHBV/PCL systems. Our theoretical results contribute to a greater physical and chemical understanding of this PHBV/PCL (25:75) blend.

2. Materials and Methods

2.1. Preparation of Biodegradable PHBV/PCL Polymeric Blends

The polymer blend was prepared with a composition of 75% PHBV (600,000 g/mol, PHB Industrial S/A, lot FE-132, Serrana SP, Brazil) and 25% PCL (2 g/mol) (50,000 g/mol, Solvay CAPA 2201 type, Brussels, Belgium) using a co-rotating twin-screw extruder (length = 40 mm and diameter = 35 mm). Thus, after extrusion, pure PHBV and the prepared PHBV/PCL (25/75) blend were injected into an Arburg Allrounder injection model 270 V 300-120 using a template for specimens according to the ASTM D-638 standard [72]. Subsequently, the samples were then exposed to γ-radiation doses (0, 50, and 100 kGy) using a Cobalt-60 multipurpose irradiator (90,000 Ci).

2.2. Characterization

The morphological analysis of these samples was conducted using an SEM microscope (PHILIPS XL-30 FEG, Hillsboro, OR, USA) with a secondary electron detector. To obtain SEM micrographs, all the samples were cryogenically fractured from ambient conditions (~20 °C and 960.7 mmHg) and coated with gold. An AT QS100 device was used to conduct DSC analysis at temperatures ranging from ambient temperature (~20 °C and 960.7 mmHg) to 200 °C with a heating rate of 20 °C/min. Analysis of the DSC curves for the raw materials of the PHBV and PCL indicated multiple melting peaks, which were consistent with the previous studies [2,21]. However, owing to the high crystallinity of these polymers and the sensitivity limitation of their DSC analysis, the determination of glass transition temperatures for the PHBV and PCL raw samples was not possible. However, in this study, to define the glass transition, we used the temperature corresponding to the peak of the tan δ (T_d) curve. This selection was made because the constant glass transition temperature value was defined by this variable, which can be obtained by the relationship with the elasticity modulus (E''/E') [73]. DMTA analysis was performed using a DMA 2980 Dynamic Mechanical Analyser (TA Instruments, Inc., New Castle, DE, USA) in the three-point bending mode, according to the ASTM D-4065-95 standard [74]. This analysis was performed at a temperature range of −80 to 40 °C, a frequency of 1 Hz, and a heating rate of 2 °C/min. Mechanical tensile tests were performed using an Instron 5500R universal testing machine with a load cell of 50 kN; an extensometer was employed to determine the elastic modulus at 0.8% strain. The distance between grips was 105 mm (10), and a rate of 100 mm/min was maintained. The tensile tests were performed with the specimen dimensions and analysis procedure specified in the ASTM D-638 standard, and the results were obtained from the average of the values corresponding to seven samples [72].

2.3. Computational Details

The theoretical models selected for this study contain polymer chains with four monomer units prepared for both pure PHBV and PCL (see Figure 1A,B). Next, based on experimental stoichiometry for PHBV/PCL blend (1:3), we have evaluated for our model all connection possibilities between these polymers, such as PHBV–PCL–PCL–PCL (de-

noted as blend BA), PCL–PHBV–PCL–PCL (denoted as blend BB), PCL–PCL–PHBV–PCL (denoted as blend BC), and PCL–PCL–PCL–PHBV (denoted as blend BD), as shown in Figure 1C–F. Although the blend structures may look symmetrical (in the case between BA and BD and between BB and BC), they are not equivalent, as is shown by the functional group connecting the fragments and their terminations (e.g., the PCL termination in BA and BD fragments are hydroxide and carbonyl groups, respectively).

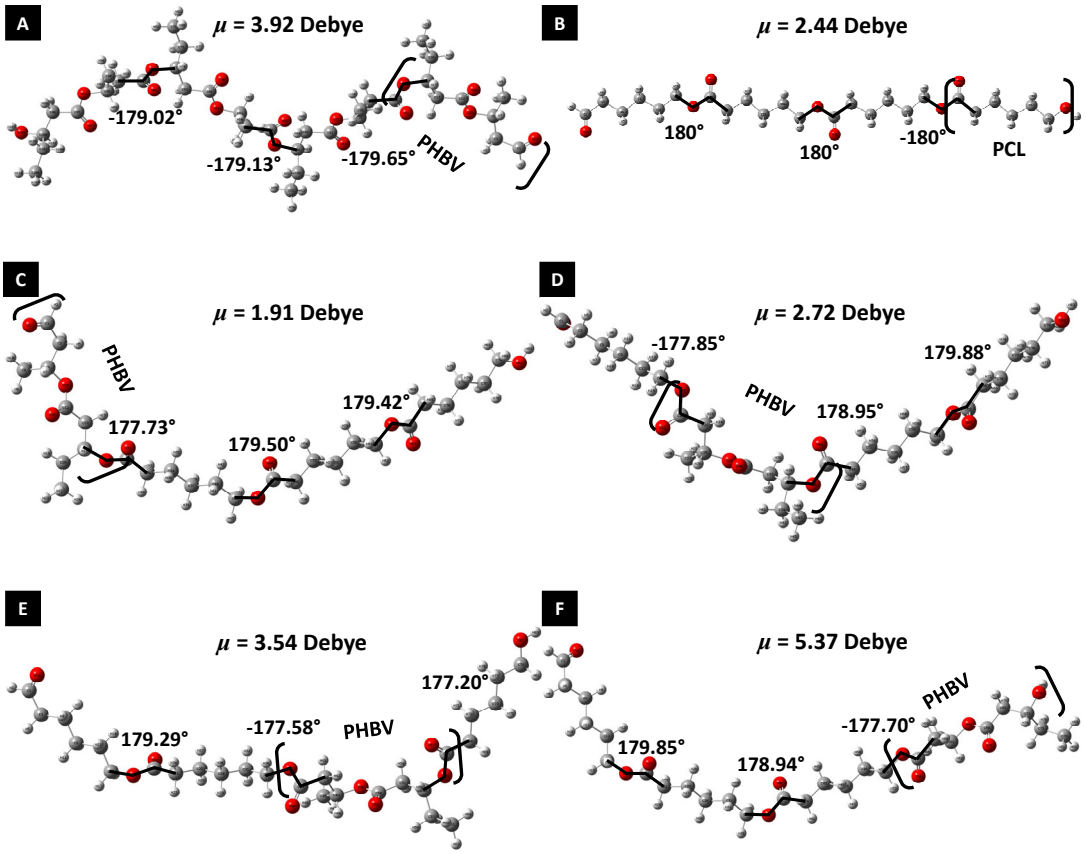

Figure 1. Optimized model structure of the polymers and blends, dihedral angles connecting PHBV and PCL fragments, and dipolar moments for (**A**) PHBV, (**B**) PCL, (**C**) BA, (**D**) BB, (**E**) BC, and (**F**) BD blends.

All of the DFT and TDDFT calculations were performed using the standard B3LYP/6-31+G(d,p) level as implemented in the Gaussian 09 package [75]. It is widely recognized that the B3LYP level can introduce errors of up to 5 kcal/mol in thermochemical energy calculations [76–79]. Full geometry optimizations and their frequencies confirmed that all models correspond to a minimum of the potential energy surface (PES). Also, ^{1}H and ^{13}C NMR calculations were performed for these structures using the gauge-including-atomic-orbital (GIAO) method, where tetramethylsilane (TMS) was used as reference [80,81]. In order to provide a better description of the electronic properties of the systems under investigation, single-point calculations at the TDDFT/B3LYP/6-31+G(d,p) level of theory were performed.

Nonconvalent interaction (NCI), electron localization function (ELF), electrostatic surface potential (ESP), NMR, and total density of states (TDOS) analyses were performed with the Multiwfn software utilizing the TDDFT checkpoint and output files [82,83]. The NCI and ESP maps were printed on Visual Molecular Dynamics (VMD) with isosurface values of 0.65 and 0.03, respectively [84]. As for the electronic properties derived from the

energies of the molecular orbitals, i.e., hardness η, softness S, Mulliken electronegativity x, and electrophilicity ω, the values were estimated by using the equations below [85].

$$\eta = \frac{1}{2}(E_{LUMO} - E_{HOMO}) \quad (1)$$

$$S = \frac{1}{\eta} \quad (2)$$

$$x = \frac{(E_{LUMO} + E_{HOMO})}{2} \quad (3)$$

$$\omega = \frac{(E_{LUMO} + E_{HOMO})^2}{2} \quad (4)$$

3. Results and Discussion

By examining the surface features of the irradiated sample using SEM micrographs, we can gain insights into how the irradiation has affected the material at the microscale. Figure 2A–C shows the SEM micrographs of PHBV/PCL polymeric blends with and without irradiation. The SEM analysis revealed that the PHBV phase in the blend exhibited distributed surface micropores. Presumably, these micropores originated during the evaporation of waste liquids (water and waste solvent), which were eliminated in processing. In the SEM micrographs of the irradiated samples, the presence of microcracks in the PHBV was observed because of the radiation effect on the splitting of the chains that weakened the polymer. Contrarily, without irradiation, the PHBV/PCL blend did not exhibit any microcracks on its structure. As a result, the extent of chain scission and the resulting weakening of the polymer will depend on the specific type of radiation used, the dose of radiation, as well as the properties of the polymer (or blend) itself. Similar results has been reported by Tubio et al. [86]. These authors also highlight the microstructure evolution in a PHBV/PCL blend with compositional variation.

Figure 2A,B shows the DSC curves for pure PHBV and PCL polymers as well as their PHBV/PCL (25:75) blend with and without irradiation, respectively. DSC results were used to determine crystalline melting temperature (Tm), enthalpy of fusion (ΔHm), and percentage of crystallinity (% C), which are summarized in Table 1. The percentages of PHBV and PCL crystallinity were calculated from the theoretical fusion heat data of the hypothetical 100% crystalline PHBV (ΔHm 100% = 146 J/g) and the hypothetical 100% crystalline PCL (ΔHm 100% = 136 J/g) [87,88]. In addition, these results suggested a small decrease in the crystalline melting temperature of the γ-irradiated PHBV/PCL blend. Therefore, the influence of irradiation on the PHBV structure resulted in the disintegration of chains instead of crosslinks, which caused an increase in the crystallinity of the pure and blend forms. In addition, the splitting occurred more frequently in large chains, which narrowed the molar mass distribution curve and shifted it to the left. This favored the order and regularity of the chains over a long range [69,89]. Contrarily, there was a significant decrease in the crystallinity of the PCL oligomer owing to the low molar mass of PCL. It was observed that under irradiation, there was a larger decrease in molar mass, as well as a clear increase in the number of very small chains, and there may have been a more favorable interaction between the blend phases. DMTA curves for the PHBV/PCL blend (with and without irradiation) are shown in Figure 2F–H. These curves indicate that the irradiation did not affect the mobility of chains in the amorphous phase. As is well known, the glass transition temperature is influenced not only by factors such as a decrease in molecular weight and polymer compatibility but also by the mobility of chains within the amorphous phase [72,89–92]. In this context, electron paramagnetic resonance (EPR) emerges as a well-established and optimal technique for studying the amorphous phase of polymers [93–95]. By determining the probe-radical correlation time, EPR offers a nuanced exploration of chain dynamics, providing a more holistic perspective on the molecular

behavior within the amorphous regions. Therefore, the use of this methodology will be the target of our future study.

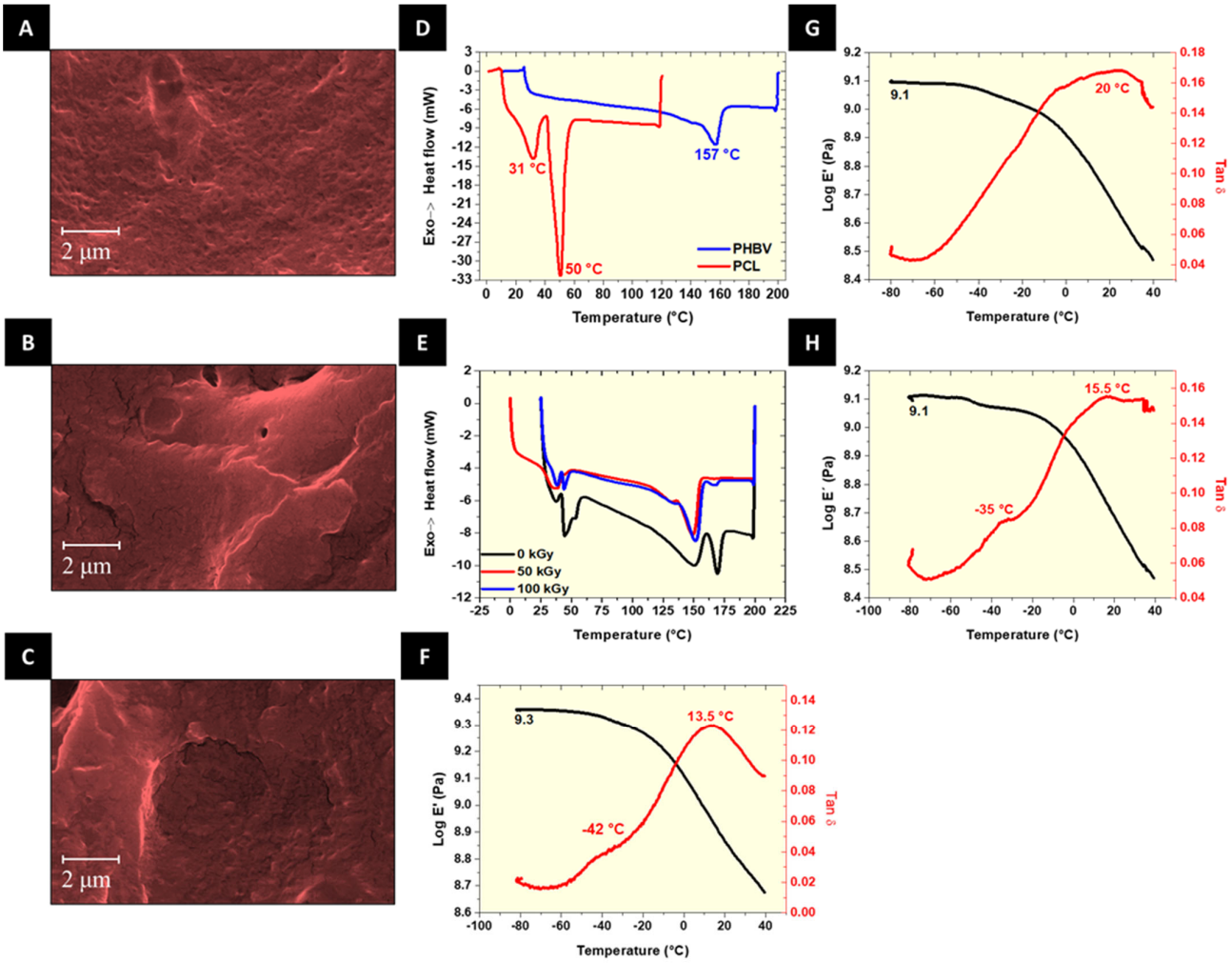

Figure 2. SEM images at 10.000 x magnification of the PHBV/PCL blend. (**A**) 0 kGy, (**B**) 50 kGy, and (**C**) 100 kGy samples. DSC curve of (**D**) both pure polymers and (**E**) their blend. The behavior of Tan δ (red) and E′ (black) due to the temperature for the PHBV/PCL blend with irradiation of (**F**) 0 kGy, (**G**) 50 kGy, and (**H**) 100 kGy.

According to the results presented in Table 1, in PHBV, rigidity and fragility were observed, which were characterized by the low deformation of the material, its sudden rupture, and the high elastic modulus. These properties were associated with the high crystallinity of PHBV [90]. Weakening of the PHBV was prolonged for some time until complete crystallization (~3 days). This phenomenon is known as the 'aging of PHBV'. It has not yet been clearly explained and has been attributed to the occurrence of secondary crystallization in the polymeric matrix [91,92]. For the PHBV/PCL blend, after irradiation, there was a slight variation in the values of the polymers' elastic moduli. The tensile strength at break significantly increased for the pure PHBV polymer. For the PHBV/PCL blend, the increase in the irradiation dose from 50 to 100 kGy caused small changes in the tensile strength; in contrast, for the pure PHBV polymer, it caused an increase in the tensile strength. All the materials suffered a significant reduction in deformation at the break with irradiation doses of 50 and 100 kGy. When compared with pure PHBV, the PHBV/PCL blend without irradiation exhibited an increase in the deformation at the break.

Table 1. Tm, ΔHm values, % of crystallinity, and tensile test results.

Materials	PHBV			PCL					
	Tm (°C)	ΔHm (J/g)	%C *	Tm (°C)	ΔHm (J/g)	%C *	Tension at Break (MPa)	Deformation at Break (%)	Elastic Modulus (GPa)
PHBV 0 kGy	157.0	39.0	26.7	-	-	-	4.2 ± 1.0	14.2 ± 2.8	0.15 ± 0.02
PHBV 50 kGy	152.5	57.0	39.0	-	-	-	11.8 ± 2.0	1.0 ± 0.1	0.10 ± 0.02
PHBV 100 kGy	156.0	43.0	29.5	-	-	-	17.8 ± 2.0	1.0 ± 0.1	0.11 ± 0.02
PHBV/PCL 0 kGy	152.0	20.0	18.3	43.0	12.0	35.3	2.0 ± 0.5	35.2 ± 5.6	0.11 ± 0.03
PHBV/PCL 50 kGy	149.0	32.0	29.2	36.0	9.0	26.5	3.9 ± 0.9	1.1 ± 0.1	0.11 ± 0.02
PHBV/PCL 100 kGy	151.0	29.0	26.5	42.0	5.0	14.7	5.7 ± 0.9	1.0 ± 0.1	0.15 ± 0.02

* Of pure polymer or normalized by the actual content of PHBV and PCL in the polymer blend.

As can clearly be seen in Figure 1, the pure PHBV polymer has a nonlinear structure due to its methyl and ethyl ramification points, while PCL presents a linear chain with alternate (zigzag) carbonyl groups and exact 180° dihedrals. This structural nonlinearity leads to an increase in the dipole moment of 2.44 Debye to 3.92 Debye for PCL and PHBV, respectively. In the case of the blend models, the exchange of a PCL monomer unit for a PHBV fragment induces a strong structural polarization, which is shown with the angle disparity between the PHBV and PCL fragments and the dihedrals diverging from the PCL by 180° around the PHBV/PCL frontier regions, likely resulting in a significant decrease in crystallinity. In this same framework, the BA blend also presents higher stability in terms of total energy, being more stable than other conformations studied exhibiting relative values of +0.32 kcal/mol compared to BB, +0.43 kcal/mol compared to BC, and +0.90 kcal/mol compared to BD.

Figure 3 depicts the ESP surface maps of pure and blend polymers, where the red and blue regions represent the negative and positive charge extremes, respectively. Looking at the PHBV surface, the negative charges are strongly centered on carbonyl oxygens, while the positive charges are localized on the hydrogens in the opposite extremity of the carbonyl group. On the other hand, the PCL polymer has negative charges which are also localized on the carbonyl oxygens and the positive charges on the hydrogens. As expected, the exchange of a PHBV unit in the PCL chain introduces extra charge concentrations around the carbonyl oxygens and hydrogens. As the PHBV fragment is dislocated between the extremities, the blend polarity is shifted due to the present groups in each extremity, which polarize the structure. Hence, the ESP surfaces are overall consistent with the dipolar moments and the total energy shift between the blends, as seen above.

Expanding the discussion regarding the pure and blend polymer structures, ^{13}C NMR and ^{1}H spectra for each system are found in Figure 4A,B. Overall, the ^{1}C NMR spectra are divided into two regions, being assigned to higher chemical shifts (160–195 ppm) within the poorly shielded carbonyl group regions and lower chemical shifts (10–80 ppm) within the strongly shielded fragments' midparts and ramifications, while this difference is more seamless for ^{1}H spectra. Therefore, due to the ramification groups in the PHBV structure, several extra signals are detected in both ^{1}H and ^{13}C NMR spectra in comparison to the PCL polymer. In particular, the peaks around 10, 20, 30, and 35 ppm in the ^{13}C spectrum are associated with the strong shielding of outer ethyl, methyl, and inner ethyl C nuclei, showing equivalent methyl nuclei and an ethyl C that is less shielded than the other fragments in the alcohol termination. The intense mode at 40 ppm is related to the shielding of C nuclei adjacent to the carbonyl groups, while the two peaks around 47 and 57 ppm belongs to nuclei between the carbonyl groups and the ethyl and methyl ramifications in the alcohol and carbonyl terminations, respectively. In the region between 65 and 90 ppm are five peaks related to the main chain C nuclei, where the modes are, respectively, associated

to the C nucleus bonded to the methyl group in the carbonyl termination (69 ppm), followed by the slightly less shielded nuclei bonded to other methyl ramifications (72 ppm), the nucleus bonded to the ethyl and the alcohol termination (74 ppm), the slightly poorly shielded C bonded to the ethyl groups (76 ppm), and the nucleus bonded to the ethyl ramification next to the carbonyl termination (77 pm). In the poorly shielded region, the mode at 166 ppm is related to the carbonyl group C between the ramifications in the carbonyl termination, followed by the peak at 168 ppm from other carbonyl C nuclei, and the last mode around 195 ppm associated with the carbonyl termination nucleus that is very poorly shielded in comparison to the alcohol termination C at 74 ppm. The same tendency is seen for the ^{1}H NMR spectrum, in which H nuclei in ramifications groups are more shielded and show chemical shifts <3 ppm, while the chain H atoms are less shielded and have shifts >3 ppm.

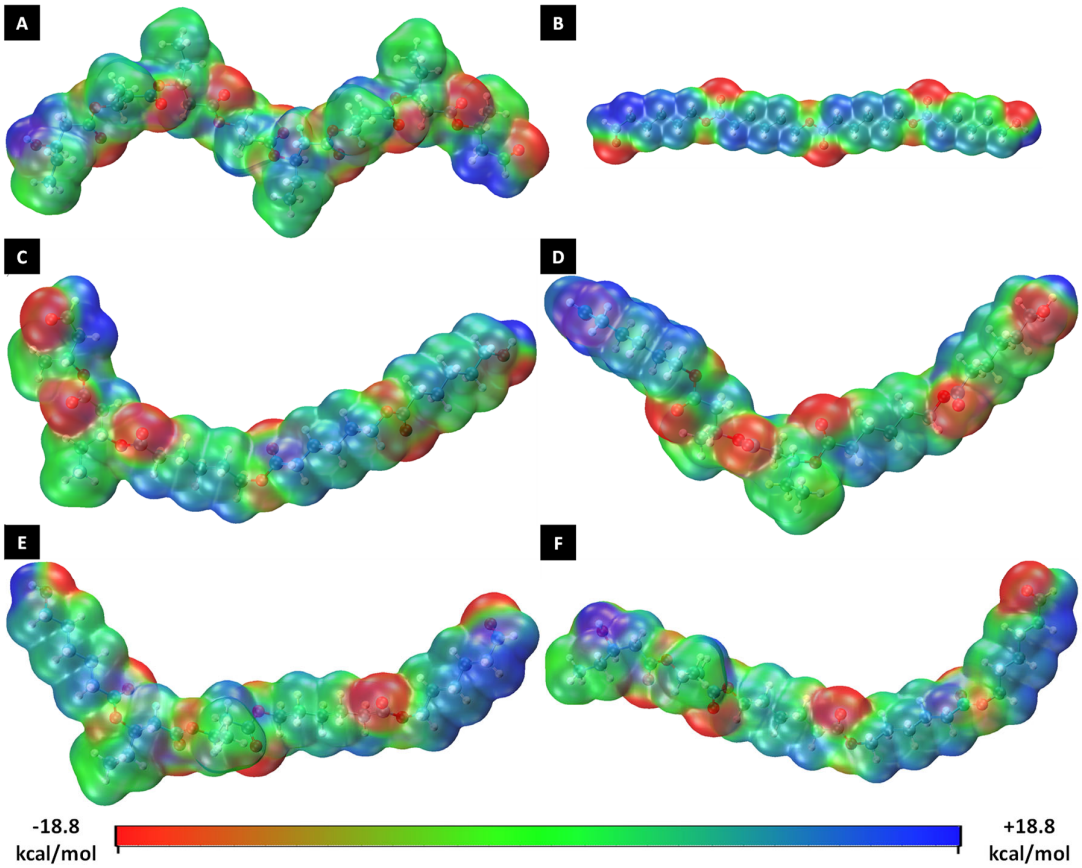

Figure 3. ESP maps of (**A**) PHBV, (**B**) PCL, (**C**) BA, (**D**) BB, (**E**) BC, and (**F**) BD.

On the other hand, the PCL polymer shows a less shielded structure than PHBV, which reflects a system more sensitive to the chemical environment due to its linear nature. As evident in the NMR spectra of PCL, due to its linear chain with no ramifications and symmetrical nuclei it can be easily distinguished from PHBV. Instead, the PCL structure has a mode around 25 ppm related to the carbonyl termination, followed by the region of 26–40 ppm with main chain C modes, which are less shielded and show higher chemical shifts as the nuclei are closer to the carbonyl groups. The peak at 50 ppm belongs to a nucleus adjacent to the carbonyl termination, while the C adjacent to the alcohol termination is found at 66 pm, and the modes at 69 ppm are associated with nuclei between C-C-O in the frontier between fragments. Like PHBV, the carbonyl nuclei are less shielded and related to three modes around 168, 169, and 170 ppm for each of the frontier regions between fragments, where the nuclei are slightly poorly shielded as they get closer to the alcohol termination, and there is the last peak around 195 ppm from the carbonyl termination.

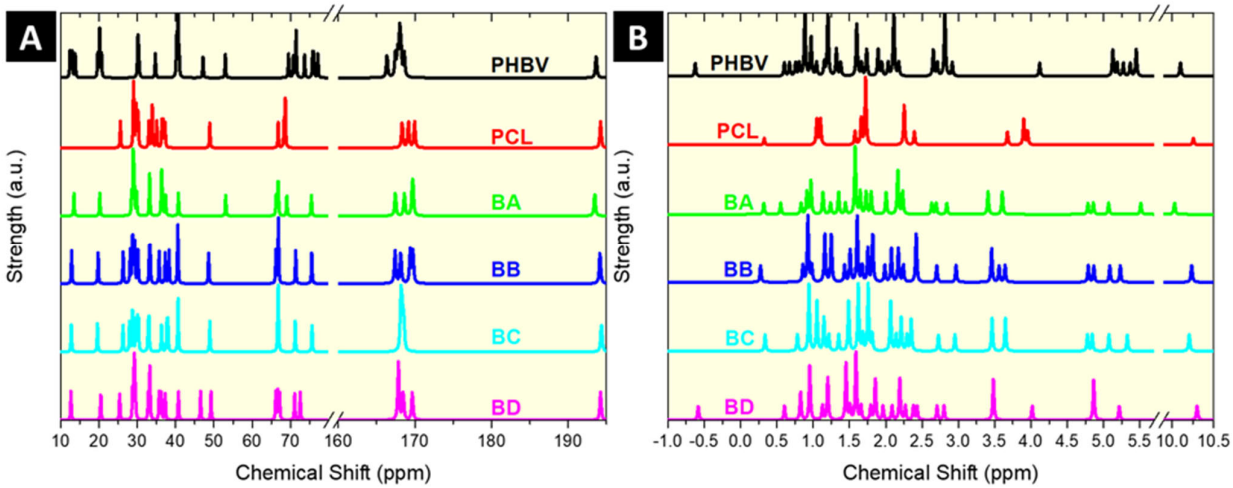

Figure 4. (**A**) ^{13}C and (**B**) ^{1}H NMR spectra of the polymers.

PCL shows a cleaner ^{1}H spectrum due to its symmetrical nature, having three pairs of H nuclei in the same axis of the frontier O nuclei, and two pairs in the opposite direction of the axis. Hence, the first mode at 0.3 ppm belongs to the alcohol H, while the peaks around 1.1, 1.7, and 2.2 are associated with nuclei in the middle of the three pairs, the opposite H pairs, and the pairs next to the carbonyl group, respectively, with the carbonyl termination lightly shifted. The peaks around 3.6 and 3.9 ppm are related to the pair next to the alcohol termination and the pairs adjacent to the frontier O nuclei, respectively. Lastly, the mode at 10.3 belongs to the poorly shielded nucleus from the carbonyl termination.

As expected, the blends show a hybrid behavior between PHBV and PCL, where the PHBV fragments have heavily shielded ramifications and decrease next to the carbonyl groups, while the PCL fragments are more shielded in the middle regions than the extremities in the fragments' frontier zones. These modes, discussed for each part of the PHBV and PCL polymers, are found in the blends' pattern, with slight shifts depending on where the PHBV–PCL frontier is present. In general, the exchange of a PCL fragment for PHBV in the polymer chain has a very low impact on the structure in terms of shielding, which, except for the BC blend and its mostly equivalent nuclei, shows a seamless difference with a chemical shift around 2 ppm for carbonyl C nuclei in the PHBV fragment. However, this small difference makes the PHBV frontier regions slightly more sensitive to the chemical environment than PCL zones. In this framework, the same tendencies observed in the ^{1}H NMR spectra of both polymers and blends can also be identified in the experimental work of Xia et al. [93], in which nuclei in the carbonyl groups show higher chemical shifts and are significantly less shielded than other regions. In addition, as clearly shown in the higher regions of the NMR spectra, nuclei in the termination parts are the least shielded for all structures, thus making the terminations the most sensitive regions with respect to the chemical environment.

A UV-vis spectrum for each polymer is found in Figure 5A. All systems have two bands, one with a higher intensity around 215 nm and the other with a lower intensity near 288 nm. The higher peak of PCL is slightly blue shifted to around 211 nm due to transitions within 195 nm. Hence, the blends have the same blue-shifted band between the PCL and PHBV positions but with lower intensities, except for the BC blend, which shows higher intensity than PCL. The excitations involved in the UV-vis peaks are characterized by electronic transitions of the following nature: HOMO-3 → LUMO+2 (5.79 eV) for PHBV, HOMO-1 → LUMO+2 (6.35 eV) for PCL, HOMO-5 → LUMO+1 (5.77 eV), HOMO-4 → LUMO+1 (5.79 eV), HOMO-2 → LUMO+5 (5.78 eV), and HOMO-1 → LUMO+1 (5.75 eV) for the BA, BB, BC, and BD blends, respectively. In the same perspective, all excitations at 288 nm are due to HOMO → LUMO (4.31 eV) electronic transitions. Our results are aligned with the experimental literature, as seen in the work of Abdelrazek et al. [94] regarding

PCL/PMMA blends, where they reported a characteristic absorption band centered around 280 nm related to carbonyl groups for pure PCL. Thus, the band described by the authors is likely caused by HOMO → LUMO transitions, while the HOMO and LUMO are indeed localized within carbonyl groups in the termination regions as shown in the MOs maps in the Supplementary Information. In addition, Nanda et al. (2011) in their work with PHBV/PLA blends also reported an absorption band around 350 nm for pure PHBV polymer, likely being related to HOMO → LUMO transitions as well [95].

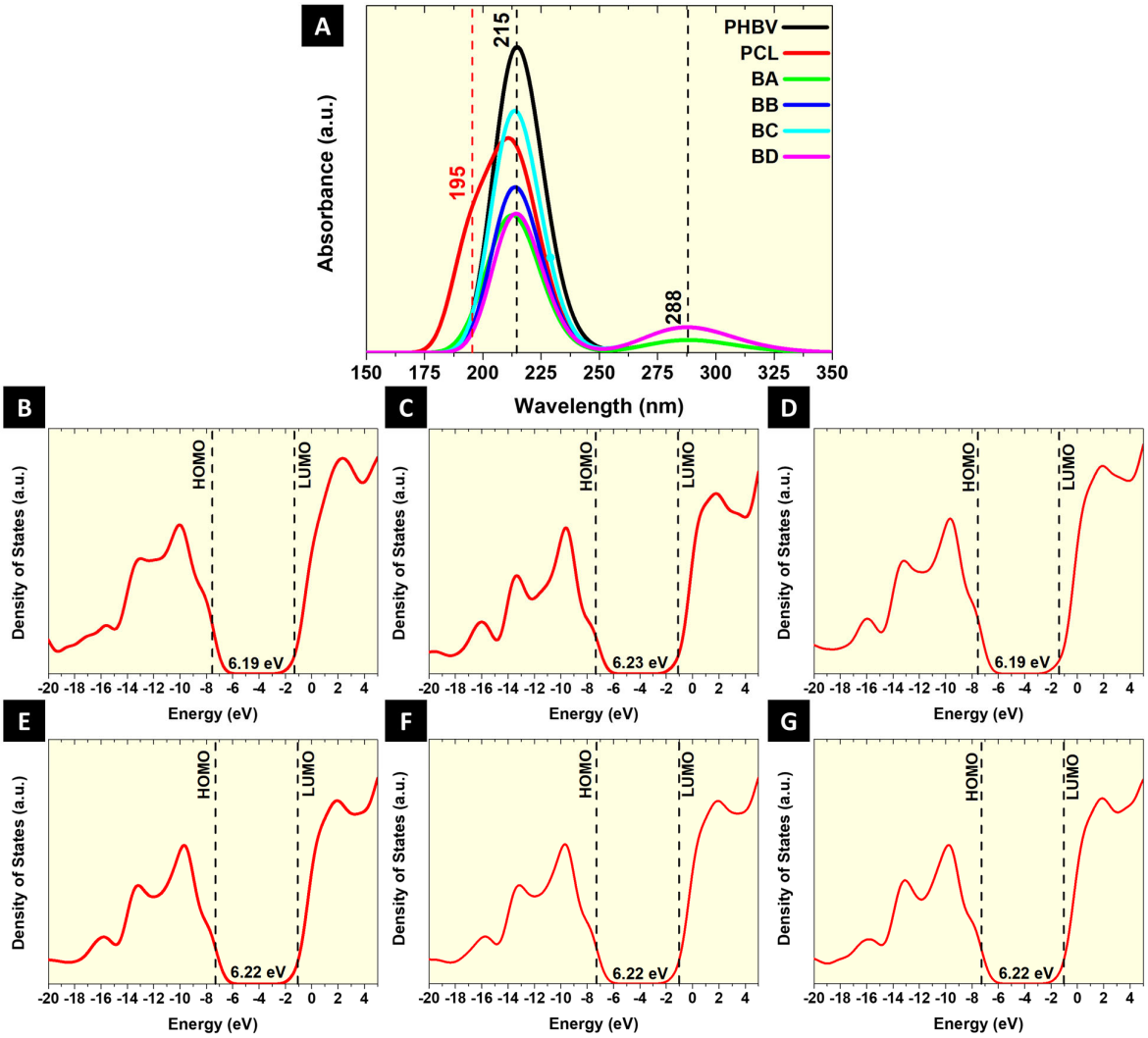

Figure 5. (**A**) UV-vis spectra of the polymers. TDOS spectra of (**B**) PHBV, (**C**) PCL, (**D**) BA, (**E**) BB, (**F**) BC, and (**G**) BD.

Figure 5B–G shows the TDOS of the polymers. As is shown in the TDOS spectra, the HOMO and LUMO have relatively low densities of states in comparison to the valence and conduction bands, which show two bands each with very high contributions, from −14 to −8 eV for the valence band, and from 0 to 5 eV for the conduction band. In general, both HOMO and LUMO are localized within the carbonyl terminations in all polymers, which HOMOs are mostly composed of *p* atomic orbitals from carbonyl O (~67%), as well as with a small contribution of *p* and *s* atomic orbitals from neighbor C (~18%) and H (~11%) nuclei, respectively. On the other hand, LUMOs show a major contribution of *p* atomic orbitals from carbonyl C (~66%) and O (~28%) nuclei, and lesser contribution of *s* atomic orbitals from H (~5%), thus in agreement with the MOs maps shown in the Supplementary Information.

Although the PHBV has a very slight band gap energy difference to PCL (0.04 eV), and the blends have a tendency of intermediate band gap between the pure polymers, the energy difference is still significantly small and within the error range of DFT approximations, in which an indication of which system has a lower or higher band gap would be inaccurate. Overall, information regarding the polymers and blend properties, such as the band gap, is very scarce, due to being very dependent on variables like molar weight. However, Abdelrazek et al. (2015) studied the spectroscopic properties of PCL polymer and derivative blends, where, in their work, a direct and indirect band gap of 4.71 eV and 4.26 eV were estimated using the Devis and Mott model, while the Tauc method reached 3.83 eV [94]. As mentioned beforehand, this high shift in the band gap is caused by the huge difference in molar weight between a PCL polymer and our model, in which the polymerization and molar weight leads to a heavy increase in intermediate states between the valence and conduction bands and the band gap decrease. In addition, despite PCL and PHBV having similar band gap values in our models, in reality the band gaps should show a significant discrepancy between these polymers because of the difference between the linear PCL and the ramified PHBV structures, having a strong influence in the polymer packing and density.

As a complement to this discussion, Table 2 lists some electronic properties derived from the HOMO and LUMO energies. As shown in the table, all values are mostly identical and with very slight shifts, such as the BA blend with properties very slightly inclined to the PHBV polymer while the BB, BC, and BD blends are more PCL alike, although the DFT error must be taken in consideration. Nonetheless, all systems show an average band gap of 6.2 eV, hardness of 3.1 eV, softness of 0.32 eV, and Muliken Electronegativity of −4.3 eV, while the electrophilicity is more sensitive to the energy values and ranges from 34.93 eV for the BC blend to 39.30 eV for BA.

Table 2. Electronic properties derived from the HOMO and LUMO energies.

Polymer.	Band Gap	Hardness	Softness	Muliken Electronegativity	Electrophilicity
PHBV	6.19	3.10	0.32	−4.42	39.06
PCL	6.23	3.11	0.32	−4.23	35.75
BA	6.19	3.10	0.32	−4.43	39.30
BB	6.22	3.11	0.32	−4.20	35.30
BC	6.22	3.11	0.32	−4.18	34.93
BD	6.22	3.11	0.32	−4.18	34.95

All units in eV.

Figure 6A–F shows the NCI maps and their respective reduced density gradient (RDG) maps, where the blue, green, and red regions represent strong interactions (i.e., hydrogen and halogen bonds), van der Waals (vdW) interactions, and strong repulsions (i.e., steric effects), respectively. NCI analysis helps in understanding the nature and strength of intermolecular interactions in complex systems [96]. In this framework, the PHBV structure (Figure 6A) has strong steric effects between the carbonyl oxygens, and weak vdW interactions between the same oxygens and the adjacent hydrogen atoms from the methyl and ethyl ramifications, contributing to a non-linear structure. On the other hand, those same interactions are of significantly lower intensity for the PCL polymer (Figure 6B), showing a structure with strong repulsions between the carbonyl oxygens in a smaller area and vdW interactions between the chain hydrogens, complementing the linear geometry. Hence, both patterns are also observed in the blends' structures, where the PCL monomer units show smaller surfaces of steric effects and vdW interactions, while the PHBV fractions have wider surfaces due to interactions with the methyl and ethyl ramifications that strongly contribute to the structural distortion and break of linearity in the PHBV/PCL boundary, as seen clearly in the BB blend (Figure 6D).

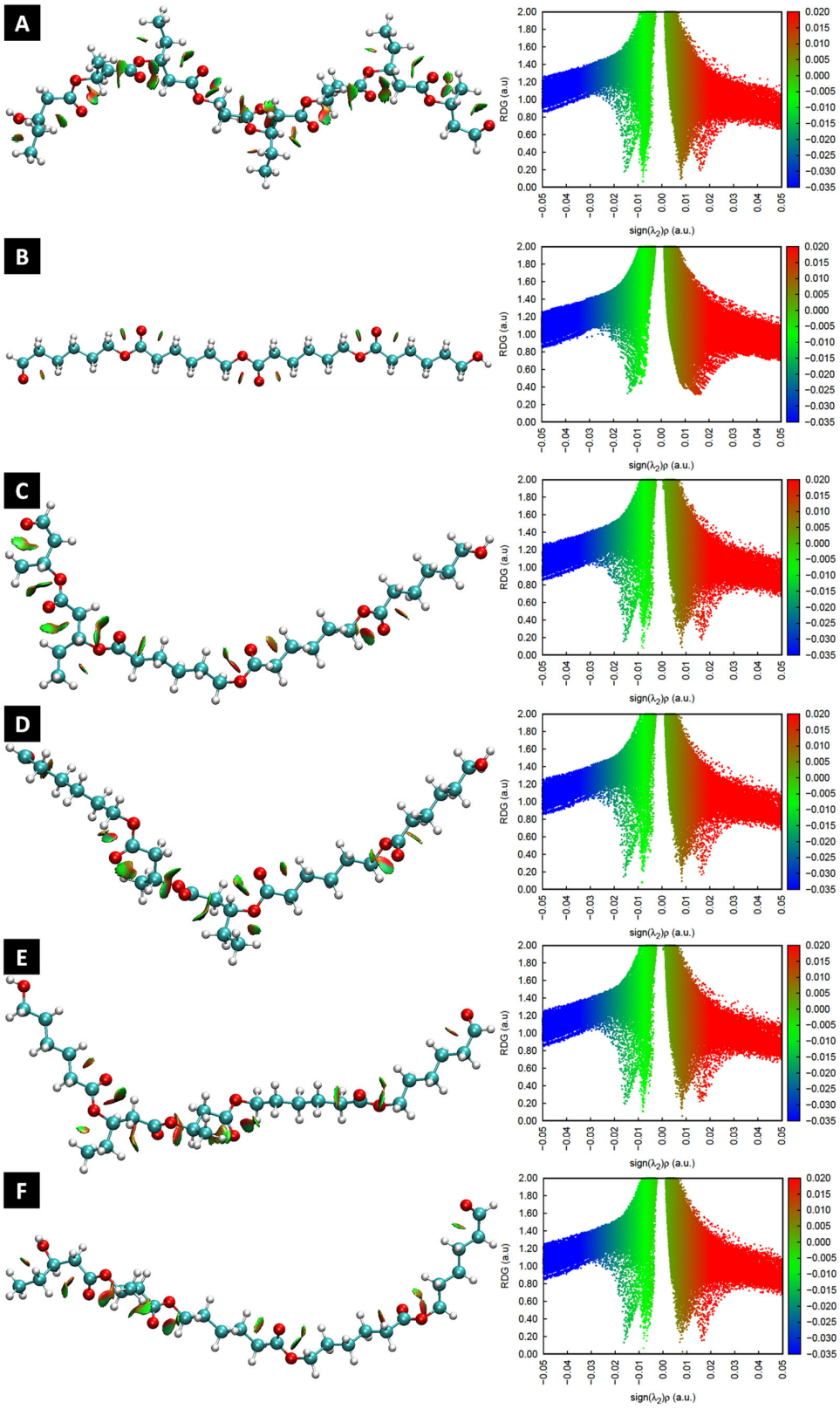

Figure 6. NCI maps with weak interactions within (**A**) PHBV, (**B**) PCL, (**C**) BA, (**D**) BB, (**E**) BC, and (**F**) BD structures.

ELF surface maps shown in Figure 7 were made from half planes cut from the X- and Y-axis with the intersection at the Z-axis origin. ELF surface maps indicate electron localization, where red values are associated with higher localization. Hence, the ELF

analysis provides insights into the bonding and delocalization of electrons in a molecular system [97]. Although the electron localization density outside of the intersecting plane is without the ELF surface range due to the nonlinear nature of the PHBV polymer (Figure 7A), there is very high electron localization around the hydrogen nuclei due to lone pairs and high localization within the oxygen nuclei valence shells and the C–C and C–O bond midpoints, while an electron-gas-like pair probability from external shells surrounds the polymer chain. In contrast, the electron localization is more clearly shown in the PCL polymer (Figure 7B) because of its linear nature, in which very high localization is seen around the terminal hydrogen nuclei due to lone pairs and high localization around the polymer chain bonding midpoints and the oxygen nuclei external shells, with wider areas on double-bonding oxygens. In the case of PCL, the localized electrons around the chain hydrogen nuclei are not as visible as in the PHBV polymer because of their angle in relation to the surface. The same patterns are observed within the blends' electron localization surfaces (Figure 7C–F) as well due to their PCL and PHBV monomer units, in which highly localized lone pairs are found on hydrogen nuclei and high localized electrons are around the oxygen nuclei valence shells and the C–C and C–O bonds midpoints.

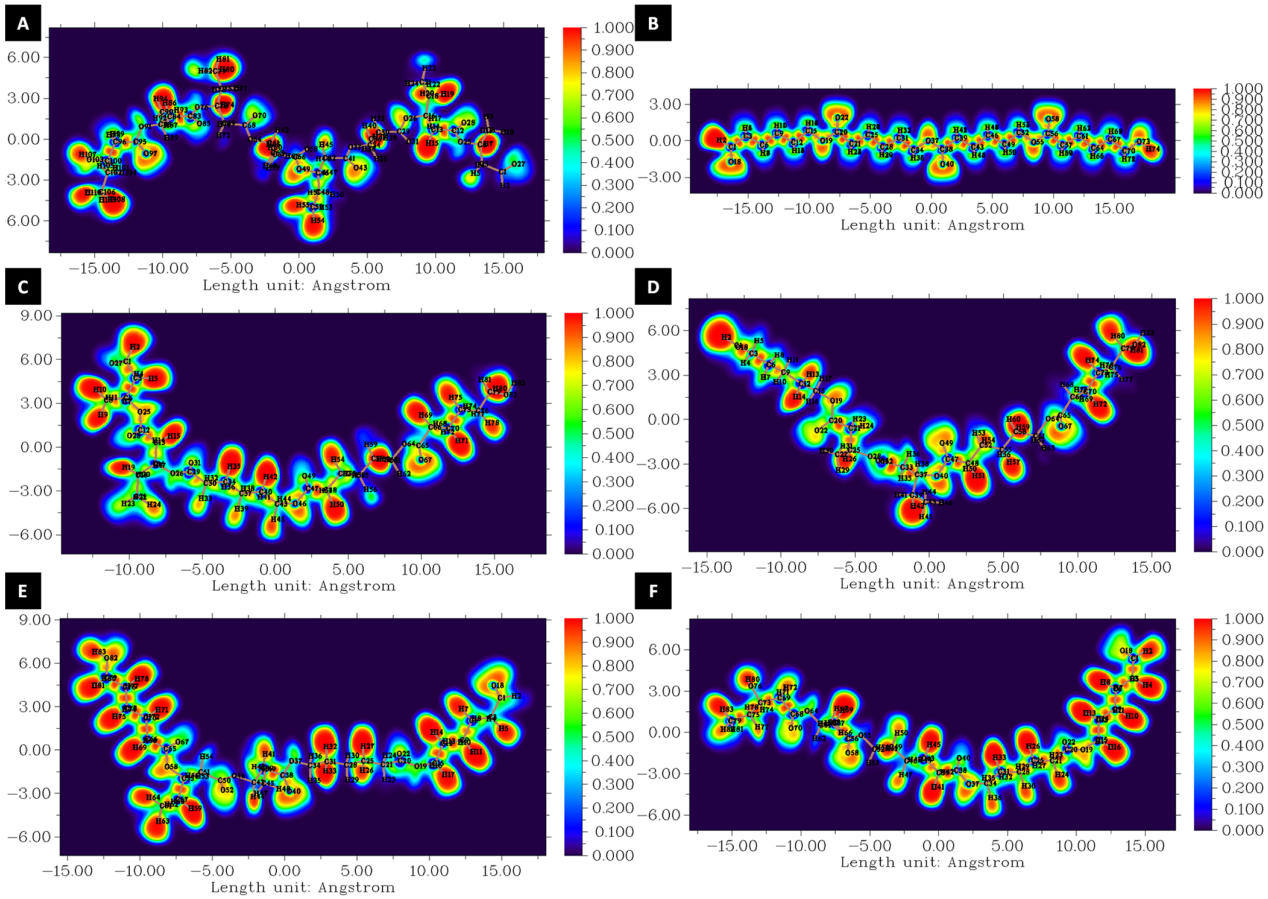

Figure 7. ELF surface maps of (**A**) PHBV, (**B**) PCL, (**C**) BA, (**D**) BB, (**E**) BC, and (**F**) BD structures.

Both NCI and ELF analyses, in general, contribute to our understanding of molecular structure and interactions of blends, that is, shedding light on the fundamental physical properties and behavior of such compounds [96–98].

4. Conclusions

In this study, we tried to evaluate the physical and mechanical properties of PHBV by simultaneous or isolated modifications based on low-molar-mass PCL at γ-irradiation doses of 50 and 100 kGy. In addition, we have used computational simulation to study the

interactions between PHBV and PCL at the molecular level, which in turn may provide relevant chemical insights into their spectroscopic and physicochemical behavior. It was concluded that the processing conducted for all materials, i.e., extrusion, drying, and injection, was adequate for providing uniform specimens. The 50 and 100 kGy irradiation doses degraded (via splitting of macromolecules) the pure polymer and the blend, as indicated by the mechanical properties (more evident from the deformation owing to the tensile strain at break). The radiation caused splitting instead of crosslinks in the polymer chains. In short, studying the effects of γ-radiation on biodegradable polymers can also help to improve our understanding of the degradation mechanisms of these PHBV/PCL materials, which can be useful in developing strategies for improving their stability and performance in the future.

Supplementary Materials: The following supporting information can be downloaded at: https://www.mdpi.com/article/10.3390/nanomanufacturing4010002/s1.

Author Contributions: F.R., J.P.A.d.J. and S.A.C.: conceptualization, methodology, software, validation, formal analysis, investigation, data curation, and writing—original draft preparation; F.R. and F.d.A.L.P.: conceptualization, resources, formal analysis, investigation, data curation, writing—review and editing, supervision, project administration, and funding acquisition. All authors have read and agreed to the published version of the manuscript.

Funding: This research did not receive any specific grant from funding agencies in the public, commercial, or not-for-profit sectors.

Data Availability Statement: Data are contained within the article.

Acknowledgments: The authors gratefully acknowledge the support from the Brazilian agencies CNPq, CAPES, and Fundação Araucária. We are also especially grateful for the computational facilities at UFLA.

Conflicts of Interest: The authors declare no conflicts of interest.

References

1. Amass, W.; Amass, A.; Tighe, B. A Review of Biodegradable Polymers: Uses, Current Developments in the Synthesis and Characterization of Biodegradable Polyesters, Blends of Biodegradable Polymers and Recent Advances in Biodegradation Studies. *Polym. Int.* **1998**, *47*, 89–144. [CrossRef]
2. Darwis, D.; Mitomo, H.; Enjoji, T.; Yoshii, F.; Makuuchi, K. Enzymatic Degradation of Radiation Crosslinked Poly(ε–Caprolactone). *Polym. Degrad. Stab.* **1998**, *62*, 259–265. [CrossRef]
3. Alaswad, S.O.; Mahmoud, A.S.; Arunachalam, P. Recent Advances in Biodegradable Polymers and Their Biological Applications: A Brief Review. *Polymers* **2022**, *14*, 4924. [CrossRef] [PubMed]
4. Alizadeh-Osgouei, M.; Li, Y.; Wen, C. A Comprehensive Review of Biodegradable Synthetic Polymer-Ceramic Composites and Their Manufacture for Biomedical Applications. *Bioact. Mater.* **2019**, *4*, 22–36. [CrossRef]
5. Yang, Z.; Nollenberger, K.; Albers, J.; Craig, D.; Qi, S. Microstructure of an Immiscible Polymer Blend and Its Stabilization Effect on Amorphous Solid Dispersions. *Mol. Pharm.* **2013**, *10*, 2767–2780. [CrossRef]
6. Korycki, A.; Garnier, C.; Abadie, A.; Nassiet, V.; Sultan, C.T.; Chabert, F. Poly(Etheretherketone)/Poly(Ethersulfone) Blends with Phenolphthalein: Miscibility, Thermomechanical Properties, Crystallization and Morphology. *Polymers* **2021**, *13*, 1466. [CrossRef]
7. Oréfice, R.L.; Pereira, M.M.; Mansur, H.S. *Biomateriais: Fundamentos e Aplicações*; Cultura Médica: Rio de Janeiro, Brazil, 2006.
8. Reinaldo, J.D.S.; Nascimento, M.C.B.C.D.; Ito, E.N.; Hage, E., Jr. Rheological, Mechanical and Morphological Properties of Poly(Methyl Methacrylate)/Poly(Ethylene Terephthalate) Blend with Dual Reactive Interfacial Compatibilization. *Polímeros* **2015**, *25*, 451–460. [CrossRef]
9. Song, R.; Murphy, M.; Li, C.; Ting, K.; Soo, C.; Zheng, Z. Current Development of Biodegradable Polymeric Materials for Biomedical Applications. *Drug Des. Devel. Ther.* **2018**, *12*, 3117–3145. [CrossRef]
10. Müller, R.-J.; Kleeberg, I.; Deckwer, W.-D. Biodegradation of polyesters containing aromatic constituents. *J. Biotechnol.* **2001**, *86*, 87–95. [CrossRef]
11. Yoshie, N.; Saito, M.; Inoue, Y. Effect of chemical compositional distribution on solid-state structures and properties of poly(3-hydroxybutyrate-co-3-hydroxyvalerate). *Polymer* **2004**, *45*, 1903–1911. [CrossRef]
12. Qiao, H.; Maazouz, A.; Lamnawar, K. Study of Morphology, Rheology, and Dynamic Properties toward Unveiling the Partial Miscibility in Poly(lactic acid)—Poly(hydroxybutyrate-co-hydroxyvalerate) Blends. *Polymers* **2022**, *14*, 5359. [CrossRef] [PubMed]
13. Maraveas, C. Production of Sustainable and Biodegradable Polymers from Agricultural Waste. *Polymers* **2020**, *12*, 1127. [CrossRef] [PubMed]

14. Pachekoski, W.M.; Agnelli, J.A.M.; Belem, L.P. Thermal, mechanical and morphological properties of poly (hydroxybutyrate) and polypropylene blends after processing. *Mater. Res.* **2009**, *12*, 159–164. [CrossRef]
15. Pesaranhajiabbas, E.; Misra, M.; Mohanty, A.K. Recent progress on biodegradable polylactic acid based blends and their biocomposites: A comprehensive review. *Int. J. Biol. Macromol.* **2023**, *253*, 126231. [CrossRef] [PubMed]
16. Goonoo, N.; Bhaw-Luximon, A.; Jhurry, D. Biodegradable polymer blends: Miscibility, physicochemical properties and biological response of scaffolds. *Polym. Int.* **2015**, *64*, 1289–1302. [CrossRef]
17. Arif, Z.U.; Khalid, M.Y.; Sheikh, M.F.; Zolfagharian, A.; Bodaghi, M. Biopolymeric sustainable materials and their emerging applications. *J. Environ. Chem. Eng.* **2022**, *10*, 108159. [CrossRef]
18. Yoshie, N.; Nakasato, K.; Fujiwara, M.; Kasuya, K.; Abe, H.; Doi, Y.; Inoue, Y. Effect of Low Molecular Weight Additives on Enzymatic Degradation of Poly(3-Hydroxybutyrate). *Polymer* **2000**, *41*, 3227–3234. [CrossRef]
19. Ibrahim, M.I.; Alsafadi, D.; Alamry, K.A.; Hussein, M.A. Properties and Applications of Poly(3-Hydroxybutyrate-Co-3-Hydroxyvalerate) Biocomposites. *J. Polym. Environ.* **2021**, *29*, 1010–1030. [CrossRef]
20. Bakare, R.A.; Bhan, C.; Raghavan, D. Synthesis and Characterization of Collagen Grafted Poly(Hydroxybutyrate–Valerate) (PHBV) Scaffold for Loading of Bovine Serum Albumin Capped Silver (Ag/BSA) Nanoparticles in the Potential Use of Tissue Engineering Application. *Biomacromolecules* **2014**, *15*, 423–435. [CrossRef]
21. Hammiche, D.; Boukerrou, A.; Ninan, N. Properties of Biocomposites Based on Poly (Hydroxybutyrate-Co-Valerate). In *AIP Conference Proceedings*; AIP Publishing: Melville, NY, USA, 2018; p. 020117.
22. Labet, M.; Thielemans, W. Synthesis of Polycaprolactone: A Review. *Chem. Soc. Rev.* **2009**, *38*, 3484. [CrossRef]
23. Sánchez-Safont, E.L.; González-Ausejo, J.; Gámez-Pérez, J.; Lagarón, J.M.; Cabedo, L. Poly(3-Hydroxybutyrate-co-3-Hydroxyvalerate)/Purified Cellulose Fiber Composites by Melt Blending: Characterization and Degradation in Composting Conditions. *J. Renew. Mater.* **2016**, *4*, 123–132. [CrossRef]
24. Balakrishna Pillai, A.; Jaya Kumar, A.; Kumarapillai, H. Biosynthesis of Poly(3-Hydroxybutyrate-Co-3-Hydroxyvalerate) (PHBV) in *Bacillus aryabhattai* and Cytotoxicity Evaluation of PHBV/Poly(Ethylene Glycol) Blends. *3 Biotech* **2020**, *10*, 32. [CrossRef] [PubMed]
25. Magalhães, N.F.; Andrade, C.T.D. Properties of Melt-Processed Poly(Hydroxybutyrate-Co-Hydroxyvalerate)/Starch 1:1 Blend Nanocomposites. *Polímeros* **2013**, *23*, 366–372. [CrossRef]
26. Policastro, G.; Panico, A.; Fabbricino, M. Improving Biological Production of Poly(3-Hydroxybutyrate-Co-3-Hydroxyvalerate) (PHBV) Co-Polymer: A Critical Review. *Rev. Environ. Sci. Bio/Technol.* **2021**, *20*, 479–513. [CrossRef]
27. Hassaini, L.; Kaci, M.; Dehouche, N.; Bruzaud, S. A Degradation Study of Poly(3-Hydroxybutyrate-Co-3-Hydroxyvalerate) and Olive Husk Flour Biocomposites under Marine Environment. *Macromol. Symp.* **2022**, *404*, 2100353. [CrossRef]
28. Rosa, D.S.; Franco, B.L.M.; Calil, M.R. Biodegradabilidade e Propriedades Mecânicas de Novas Misturas Poliméricas. *Polímeros* **2001**, *11*, 82–88. [CrossRef]
29. Phukon, P.; Saikia, J.P.; Konwar, B.K. Bio-Plastic (P-3HB-Co-3HV) from *Bacillus circulans* (MTCC 8167) and Its Biodegradation. *Colloids Surf. B Biointerfaces* **2012**, *92*, 30–34. [CrossRef] [PubMed]
30. Kaniuk, Ł.; Podborska, A.; Stachewicz, U. Enhanced Mechanical Performance and Wettability of PHBV Fiber Blends with Evening Primrose Oil for Skin Patches Improving Hydration and Comfort. *J. Mater. Chem. B* **2022**, *10*, 1763–1774. [CrossRef]
31. Bittolo Bon, S.; Chiesa, I.; Morselli, D.; Degli Esposti, M.; Fabbri, P.; De Maria, C.; Foggi Viligiardi, T.; Morabito, A.; Giorgi, G.; Valentini, L. Printable Smart 3D Architectures of Regenerated Silk on Poly(3-Hydroxybutyrate-Co-3-Hydroxyvalerate). *Mater. Des.* **2021**, *201*, 109492. [CrossRef]
32. Singh, S.; Ghosh, C.; Roy, P.; Pal, K. Biosynthesis of Folic Acid Appended PHBV Modified Copper Oxide Nanorods for PH Sensitive Drug Release in Targeted Breast Cancer Therapy. *Int. J. Pharm.* **2022**, *622*, 121831. [CrossRef]
33. Rodrigues, A.A.; Batista, N.A.; Malmonge, S.M.; Casarin, S.A.; Agnelli, J.A.M.; Santos, A.R.; Belangero, W.D. Osteogenic Differentiation of Rat Bone Mesenchymal Stem Cells Cultured on Poly (Hydroxybutyrate-Co-Hydroxyvalerate), Poly (ε-Caprolactone) Scaffolds. *J. Mater. Sci. Mater. Med.* **2021**, *32*, 138. [CrossRef] [PubMed]
34. Baqeri, N.; Shahsavari, S.; Dahouee, I.A.; Shirmard, L.R. Design of Slow-Release Methotrexate Drug Delivery System Using PHBV Magnetic Nanoparticles and Evaluation of Its Cytotoxicity. *J. Drug Deliv. Sci. Technol.* **2022**, *77*, 103854. [CrossRef]
35. Kaniuk, Ł.; Stachewicz, U. Development and Advantages of Biodegradable PHA Polymers Based on Electrospun PHBV Fibers for Tissue Engineering and Other Biomedical Applications. *ACS Biomater. Sci. Eng.* **2021**, *7*, 5339–5362. [CrossRef] [PubMed]
36. Qahtani, M.; Wu, F.; Misra, M.; Gregori, S.; Mielewski, D.F.; Mohanty, A.K. Experimental Design of Sustainable 3D-Printed Poly(Lactic Acid)/Biobased Poly(Butylene Succinate) Blends via Fused Deposition Modeling. *ACS Sustain. Chem. Eng.* **2019**, *7*, 14460–14470. [CrossRef]
37. Arif, Z.U.; Khalid, M.Y.; Noroozi, R.; Hossain, M.; Shi, H.H.; Tariq, A.; Ramakrishna, S.; Umer, R. Additive Manufacturing of Sustainable Biomaterials for Biomedical Applications. *Asian J. Pharm. Sci.* **2023**, *18*, 100812. [CrossRef] [PubMed]
38. Sá, M.L.D.; Carvalho, É.M.D.; Calvacante, J.; Araque, L.M.; Reis Sobrinho, J.F.; Barbosa, R.; Alves, T.S. Biodegradation of Poly (3-Hydroxybutyrate)/Eggshellsystems. *Mater. Res.* **2018**, *21*. [CrossRef]
39. Ma, W.; Wang, J.; Li, Y.; Yin, L.; Wang, X. Poly(3-Hydroxybutyrate-Co-3-Hydroxyvalerate) Co-Produced with l-Isoleucine in Corynebacterium Glutamicum WM001. *Microb. Cell Fact.* **2018**, *17*, 93. [CrossRef] [PubMed]

40. El-Hadi, A.; Schnabel, R.; Straube, E.; Müller, G.; Henning, S. Correlation between Degree of Crystallinity, Morphology, Glass Temperature, Mechanical Properties and Biodegradation of Poly (3-Hydroxyalkanoate) PHAs and Their Blends. *Polym. Test.* **2002**, *21*, 665–674. [CrossRef]
41. Vinhas, G.M.; Almeida, Y.M.B.D.; Lima, M.A.G.D.A.; Santos, L.A. Estudo Das Propriedades e Biodegradabilidade de Blendas de Poliéster/Amido Submetidas Ao Ataque Microbiano. *Quim. Nova* **2007**, *30*, 1584–1588. [CrossRef]
42. Imre, B.; Pukánszky, B. Compatibilization in Bio-Based and Biodegradable Polymer Blends. *Eur. Polym. J.* **2013**, *49*, 1215–1233. [CrossRef]
43. Samir, A.; Ashour, F.H.; Hakim, A.A.A.; Bassyouni, M. Recent Advances in Biodegradable Polymers for Sustainable Applications. *Npj Mater. Degrad.* **2022**, *6*, 68. [CrossRef]
44. Kumar, R.; Sadeghi, K.; Jang, J.; Seo, J. Mechanical, Chemical, and Bio-Recycling of Biodegradable Plastics: A Review. *Sci. Total Environ.* **2023**, *882*, 163446. [CrossRef] [PubMed]
45. Vroman, I.; Tighzert, L. Biodegradable Polymers. *Materials* **2009**, *2*, 307–344. [CrossRef]
46. Nakajima-Kambe, T.; Edwinoliver, N.G.; Maeda, H.; Thirunavukarasu, K.; Gowthaman, M.K.; Masaki, K.; Mahalingam, S.; Kamini, N.R. Purification, Cloning and Expression of an Aspergillus Niger Lipase for Degradation of Poly(Lactic Acid) and Poly(ε-Caprolactone). *Polym. Degrad. Stab.* **2012**, *97*, 139–144. [CrossRef]
47. Sahu, S.; Kaur, A.; Khatri, M.; Singh, G.; Arya, S.K. A Review on Cutinases Enzyme in Degradation of Microplastics. *J. Environ. Manag.* **2023**, *347*, 119193. [CrossRef]
48. Shi, K.; Jing, J.; Song, L.; Su, T.; Wang, Z. Enzymatic Hydrolysis of Polyester: Degradation of Poly(ε-Caprolactone) by *Candida antarctica* Lipase and *Fusarium solani* Cutinase. *Int. J. Biol. Macromol.* **2020**, *144*, 183–189. [CrossRef]
49. Feng, S.; Yue, Y.; Chen, J.; Zhou, J.; Li, Y.; Zhang, Q. Biodegradation Mechanism of Polycaprolactone by a Novel Esterase MGS0156: A QM/MM Approach. *Environ. Sci. Process. Impacts* **2020**, *22*, 2332–2344. [CrossRef]
50. Erdal, N.B.; Lando, G.A.; Yadav, A.; Srivastava, R.K.; Hakkarainen, M. Hydrolytic Degradation of Porous Crosslinked Poly(ε-Caprolactone) Synthesized by High Internal Phase Emulsion Templating. *Polymers* **2020**, *12*, 1849. [CrossRef]
51. Heimowska, A.; Morawska, M.; Bocho-Janiszewska, A. Biodegradation of Poly(ε-Caprolactone) in Natural Water Environments. *Polish J. Chem. Technol.* **2017**, *19*, 120–126. [CrossRef]
52. Sreeja, S.D.; Sailaja, G.S. In Vitro Osteogenic Differentiation and Biomineralization Facet of Phosphorylated Porous Poly(3-Hydroxybutyrate-Co-3-Hydroxyvalerate)/Poly(ε-Caprolactone): An Osteogenic Platform for Regenerative Bone Tissue Engineering. *ACS Appl. Polym. Mater.* **2023**, *5*, 8270–8283. [CrossRef]
53. Saudi, S.; Jun, S.; Fialkova, S.; Surendran, V.; Chandrasekaran, A.; Bhattarai, S.R.; Sankar, J.; Bhattarai, N. Incorporating Nanoconfined Chitin-Fibrils in Poly (ε-caprolactone) Membrane Scaffolds Improves Mechanical and Chemical Properties for Biomedical Application. *J. Biomed. Mater. Res. Part A* **2023**, *111*, 1185–1199. [CrossRef] [PubMed]
54. Espinoza, S.M.; Patil, H.I.; San Martin Martinez, E.; Casañas Pimentel, R.; Ige, P.P. Poly-ε-Caprolactone (PCL), a Promising Polymer for Pharmaceutical and Biomedical Applications: Focus on Nanomedicine in Cancer. *Int. J. Polym. Mater. Polym. Biomater.* **2020**, *69*, 85–126. [CrossRef]
55. Mohamed, R.M.; Yusoh, K. A Review on the Recent Research of Polycaprolactone (PCL). *Adv. Mater. Res.* **2015**, *1134*, 249–255. [CrossRef]
56. Oluwabunmi, K.E.; Zhao, W.; D'Souza, N.A. Carbon Capture Utilization for Biopolymer Foam Manufacture: Thermal, Mechanical and Acoustic Performance of PCL/PHBV CO_2 Foams. *Polymers* **2021**, *13*, 2559. [CrossRef] [PubMed]
57. Adams, B.; Abdelwahab, M.; Misra, M.; Mohanty, A.K. Injection-Molded Bioblends from Lignin and Biodegradable Polymers: Processing and Performance Evaluation. *J. Polym. Environ.* **2018**, *26*, 2360–2373. [CrossRef]
58. Voronova, M.I.; Gurina, D.L.; Surov, O.V. Properties of Poly(3-Hydroxybutyrate-Co-3-Hydroxyvalerate)/Polycaprolactone Polymer Mixtures Reinforced by Cellulose Nanocrystals: Experimental and Simulation Studies. *Polymers* **2022**, *14*, 340. [CrossRef]
59. Liu, H.; Gao, Z.; Hu, X.; Wang, Z.; Su, T.; Yang, L.; Yan, S. Blending Modification of PHBV/PCL and Its Biodegradation by Pseudomonas Mendocina. *J. Polym. Environ.* **2017**, *25*, 156–164. [CrossRef]
60. Nevoralová, M.; Koutný, M.; Ujčić, A.; Starý, Z.; Šerá, J.; Vlková, H.; Šlouf, M.; Fortelný, I.; Kruliš, Z. Structure Characterization and Biodegradation Rate of Poly(ε-Caprolactone)/Starch Blends. *Front. Mater.* **2020**, *7*, 141. [CrossRef]
61. Leja, K.; Lewandowicz, G. Polymer Biodegradation and Biodegradable Polymers—A Review. *Polish J. Environ. Stud.* **2010**, *19*, 255–266.
62. Hu, J.-Z.; Zhou, Y.-C.; Huang, L.-H.; Lu, H.-B. Development of Biodegradable Polycaprolactone Film as an Internal Fixation Material to Enhance Tendon Repair: An in Vitro Study. *BMC Musculoskelet. Disord.* **2013**, *14*, 246. [CrossRef]
63. Akter, N.; Khan, R.A.; Salmieri, S.; Sharmin, N.; Dussault, D.; Lacroix, M. Fabrication and Mechanical Characterization of Biodegradable and Synthetic Polymeric Films: Effect of Gamma Radiation. *Radiat. Phys. Chem.* **2012**, *81*, 995–998. [CrossRef]
64. Elsawy, M.A.; Fekry, M.; Sayed, A.M.; Maziad, N.A.; Saad, G.R. Physico-Chemical Characteristics of Biodegradable Poly(Lactic Acid) and Poly(Lactic Acid)/Chitosan Nano-Composites Under the Influence of Gamma Irradiation. *J. Polym. Environ.* **2023**, *31*, 2705–2714. [CrossRef]
65. Gandhi, K.; Kriz, D.; Salovey, R.; Narkis, M.; Wallerstein, R. Crosslinking of Polycaprolactone in the Pre-Gelation Region. *Polym. Eng. Sci.* **1988**, *28*, 1484–1490. [CrossRef]
66. Naikwadi, A.T.; Sharma, B.K.; Bhatt, K.D.; Mahanwar, P.A. Gamma Radiation Processed Polymeric Materials for High Performance Applications: A Review. *Front. Chem.* **2022**, *10*, 837111. [CrossRef] [PubMed]

67. Shiroud Heidari, B.; Ruan, R.; Vahabli, E.; Chen, P.; De-Juan-Pardo, E.M.; Zheng, M.; Doyle, B. Natural, Synthetic and Commercially-Available Biopolymers Used to Regenerate Tendons and Ligaments. *Bioact. Mater.* **2023**, *19*, 179–197. [CrossRef] [PubMed]
68. Oliveira, L.M.; Araujo, P.L.B.; Araujo, E.S. The Effect of Gamma Radiation on Mechanical Properties of Biodegradable Polymers Poly(3-Hydroxybutyrate) and Poly(3-Hydroxybutyrate-Co-3-Hydroxyvalerate). *Mater. Res.* **2012**, *16*, 195–203. [CrossRef]
69. Rosário, F.; Corradini, E.; Casarin, S.A.; Agnelli, J.A.M. Effect of Gamma Radiation on the Properties of Poly(3-Hydroxybutyrate-Co-3-Hydroxyvalerate)/Poly(ε-Caprolactone) Blends. *J. Polym. Environ.* **2013**, *21*, 789–794. [CrossRef]
70. Yang, H.; Liu, J. Thermal Analysis of Poly(3-Hydroxybutyrate-Co-3-Hydroxyvalerate) Irradiated under Vacuum. *Polym. Int.* **2004**, *53*, 1677–1681. [CrossRef]
71. Luk, J.Z.; Rondeau, E.; Trau, M.; Cooper-White, J.; Grøndahl, L. Characterisation of Amine Functionalised Poly(3-Hydroxybuturate-Co-3-Hydroxyvalerate) Surfaces. *Polymer* **2011**, *52*, 3251–3258. [CrossRef]
72. *ASTM ASTM D 638-02*; Standard Test Method for Tensile Properties of Plastics. ASTM: West Conshohocken, PA, USA, 2002.
73. Canevarolo, S.V., Jr. (Ed.) *Técnicas de Caracterização de Polímeros*; Artliber Editora Ltda: São Paulo, Brazil, 2004.
74. *ASTM ASTM D 4065-95*; Standard Practice for Determining and Reporting Dynamic Mechanical Properties of Plastics. ASTM: West Conshohocken, PA, USA, 1995.
75. Frisch, M.J.; Trucks, G.W.; Schlegel, H.B.; Scuseria, G.E.; Robb, M.; Cheeseman, J.; Scalmani, G.; Barone, V.; Mennucci, B.; Petersson, G.A.; et al. *Gaussian 09 (Revision A02)*; Gaussian Inc.: Wallingford, CT, USA, 2009.
76. Sousa, S.F.; Fernandes, P.A.; Ramos, M.J. General Performance of Density Functionals. *J. Phys. Chem. A* **2007**, *111*, 10439–10452. [CrossRef]
77. Legge, F.S.; Nyberg, G.L.; Peel, J.B. DFT Calculations for Cu-, Ag-, and Au-Containing Molecules. *J. Phys. Chem. A* **2001**, *105*, 7905–7916. [CrossRef]
78. Ody, K.S.; de Jesus, J.P.A.; Cava, C.E.; Albuquerque, A.R.; Maia, A.S.; Sambrano, J.R.; La Porta, F.A. Avaliação da Estrutura Eletrônica da Fase Monoclinica do Óxido de Nióbio com Base no uso de Diferentes Funcionais de Densidade. *Quim. Nova* **2021**, *44*, 1124–1131. [CrossRef]
79. Jiménez-Hoyos, C.A.; Janesko, B.G.; Scuseria, G.E. Evaluation of Range-Separated Hybrid Density Functionals for the Prediction of Vibrational Frequencies, Infrared Intensities, and Raman Activities. *Phys. Chem. Chem. Phys.* **2008**, *10*, 6621. [CrossRef] [PubMed]
80. Wolinski, K.; Hinton, J.F.; Pulay, P. Efficient Implementation of the Gauge-Independent Atomic Orbital Method for NMR Chemical Shift Calculations. *J. Am. Chem. Soc.* **1990**, *112*, 8251–8260. [CrossRef]
81. Ditchfield, R. Self-Consistent Perturbation Theory of Diamagnetism. *Mol. Phys.* **1974**, *27*, 789–807. [CrossRef]
82. Lu, T.; Chen, F. Multiwfn: A Multifunctional Wavefunction Analyzer. *J. Comput. Chem.* **2012**, *33*, 580–592. [CrossRef] [PubMed]
83. Lu, T.; Chen, F. Quantitative Analysis of Molecular Surface Based on Improved Marching Tetrahedra Algorithm. *J. Mol. Graph. Model.* **2012**, *38*, 314–323. [CrossRef]
84. Humphrey, W.; Dalke, A.; Schulten, K. VMD: Visual Molecular Dynamics. *J. Mol. Graph.* **1996**, *14*, 33–38. [CrossRef]
85. de Jesus, J.P.A.; Assis, L.C.; de Castro, A.A.; da Cunha, E.F.F.; Nepovimova, E.; Kuca, K.; de Castro Ramalho, T.; La Porta, F.A. Effect of Drug Metabolism in the Treatment of SARS-CoV-2 from an Entirely Computational Perspective. *Sci. Rep.* **2021**, *11*, 19998. [CrossRef]
86. Tubio, C.R.; Valle, X.; Carvalho, E.; Moreira, J.; Costa, P.; Correia, D.M.; Lanceros-Mendez, S. Poly(3-hydroxybutyrate-co-3-hydroxyvalerate) Blends with Poly(caprolactone) and Poly(lactic acid): A Comparative Study. *Polymers* **2023**, *15*, 4566. [CrossRef]
87. Barham, P.J.; Keller, A. The Relationship between Microstructure and Mode of Fracture in Polyhydroxybutyrate. *J. Polym. Sci. Part B Polym. Phys.* **1986**, *24*, 69–77. [CrossRef]
88. Avella, M.; Errico, M.E.; Rimedio, R.; Sadocco, P. Preparation of Biodegradable Polyesters/High-Amylose-Starch Composites by Reactive Blending and Their Characterization. *J. Appl. Polym. Sci.* **2002**, *83*, 1432–1442. [CrossRef]
89. Yoshii, F.; Darwis, D.; Mitomo, H.; Makuuchi, K. Crosslinking of Poly(ε-Caprolactone) by Radiation Technique and Its Biodegradability. *Radiat. Phys. Chem.* **2000**, *57*, 417–420. [CrossRef]
90. Sharma, R.; Ray, A.R. Polyhydroxybutyrate, Its Copolymers and Blends. *J. Macromol. Sci. Part C Polym. Rev.* **1995**, *35*, 327–359. [CrossRef]
91. Aref-Azar, A.; Biddlestone, F.; Hay, J.N.; Haward, R.N. The Effect of Physical Ageing on the Properties of Poly(Ethylene Terephthalate). *Polymer* **1983**, *24*, 1245–1251. [CrossRef]
92. Biddlestone, F.; Harris, A.; Hay, J.N.; Hammond, T. The Physical Ageing of Amorphous Poly(Hydroxybutyrate). *Polym. Int.* **1996**, *39*, 221–229. [CrossRef]
93. Xia, S.; Shen, Y.; Zhou, Y.; Yao, P.; Liu, Q.; Deng, B. Biodegradable Multiblock Copolymers Containing Poly[(3-Hydroxybutyrate)-Co-(3-Hydroxyvalerate)], Poly(ε-Caprolactone), and Polyhedral Oligomeric Silsesquioxane: Synthesis, Characterization, and Tensile Property. *Colloid Polym. Sci.* **2018**, *296*, 1667–1677. [CrossRef]
94. Abdelrazek, E.M.; Hezma, A.M.; El-khodary, A.; Elzayat, A.M. Spectroscopic Studies and Thermal Properties of PCL/PMMA Biopolymer Blend. *Egypt. J. Basic Appl. Sci.* **2016**, *3*, 10–15. [CrossRef]
95. Nanda, M.R.; Misra, M.; Mohanty, A.K. The Effects of Process Engineering on the Performance of PLA and PHBV Blends. *Macromol. Mater. Eng.* **2011**, *296*, 719–728. [CrossRef]

96. Johnson, E.R.; Keinan, S.; Mori-Sánchez, P.; Contreras-García, J.; Cohen, A.J.; Yang, W. Revealing Noncovalent Interactions. *J. Am. Chem. Soc.* **2010**, *132*, 6498–6506. [CrossRef]
97. Silvi, B.; Savin, A. Classification of Chemical Bonds Based on Topological Analysis of Electron Localization Functions. *Nature* **1994**, *371*, 683–686. [CrossRef]
98. Cormanich, R.A.; Santiago, R.T.; La Porta, F.A.; Freitas, M.P.; Rittner, R.; da Cunha, E.F.F.; Andres, J.; Longo, E.; Ramalho, T.C. Quantum chemical topological analysis of hydrogen bonding in HX. . .HX and CH3X. . .HX dimers (X = Br, Cl, F). Molecular Simulation. *Mol. Simul.* **2015**, *41*, 600–609. [CrossRef]